Catalysts **2015**, *5*, 1375-1387; doi:10.3390/catal5031375

OPEN ACCESS

catalysts

ISSN 2073-4344

www.mdpi.com/journal/catalysts

Article

Simple Preparation of Pd Core Nanoparticles for Pd Core/Pt Shell Catalyst and Evaluation of Activity and Durability for Oxygen Reduction Reaction

Hiroshi Inoue *, Ryotaro Sakai, Taiki Kuwahara, Masanobu Chiku and Eiji Higuchi

Department of Applied Chemistry, Graduate School of Engineering, Osaka Prefecture University, Sakai, Osaka 599-8531, Japan; E-Mails: s.ryotaro11@gmail.com (R.S.); su108024@edu.osakafu-u.ac.jp (T.K.); chiku@chem.osakafu-u.ac.jp (M.C.); e-higuchi@chem.osakafu-u.ac.jp (E.H.)

* Author to whom correspondence should be addressed; E-Mail: inoue-h@chem.osakafu-u.ac.jp; Tel./Fax: +81-72-254-9283.

Academic Editor: Minhua Shao

Received: 18 May 2015 / Accepted: 18 July 2015 / Published: 28 July 2015

Abstract: Pd core nanoparticles less than 5 nm in mean size were prepared on carbon black (CB) without any stabilizer by using palladium acetate as a precursor and CO as a reducing agent, and then used for preparing Pd core/Pt shell nanoparticles-loaded CB (Pt/Pd/CB). The mean size of Pd nanoparticles could be controlled by the concentration of palladium acetate and the CO bubbling time. The cyclic voltammograms of two Pd nanoparticles-loaded CB ($Pd_{4.2}$/CB, $Pd_{3.3}$/CB) electrodes whose mean size was 4.2 and 3.3 nm, respectively, had characteristics similar to a Pt electrode after the formation of a Pt monolayer shell, suggesting that the Pd core nanoparticles were almost covered with the Pt monolayer shell. The oxygen reduction reaction (ORR) on both Pt/Pd/CB proceeded in 4-electron reduction mechanism. Both Pt/Pd/CB electrodes was *ca.* 1.5 times higher in ORR activity per electrochemical surface area of Pt (specific activity, SA) than the commercial Pt nanoparticles-loaded CB (Tanaka Kikinzoku Kogyo, Pt/CB-TKK) electrode, and the Pt/$Pd_{3.3}$/CB electrode had higher SA than the Pt/$Pd_{4.2}$/CB electrode. The ORR activity per unit mass of Pt for both Pt/Pd/CB electrodes was 5.0 and 5.5 times as high as that for the Pt/CB-TKK electrode, respectively. The durability of both Pt/Pd/CB electrodes was comparable to that of Pt/CB-TKK.

Keywords: oxygen reduction reaction; Pd nanoparticle; Pd core/Pt shell; carbon monoxide

1. Introduction

Polymer electrolyte fuel cells (PEFCs) attract great attention as a clean power source for habitations and electric vehicles due to their high energy conversion efficiency, low emission of pollutants and low operating temperature. However, a serious issue for their practical use is high price of Pt, which has the highest activity for oxygen reduction reaction (ORR) at the cathode, so reducing the consumption of Pt is an urgent mission. For this purpose, various strategies including the preparation of nanoparticles of various Pt-based alloys and bimetals have been attempted so far [1–8].

It is well-known that only a few surface atomic layers of catalyst participate in heterogeneous catalysis, suggesting that covering foreign metal core nanoparticles with a Pt monolayer shell is the most effective way to reduce the Pt consumption with keeping the ORR activity because the Pt utilization is ultimately enhanced. This can be another desirable strategy. For realizing the formation of a Pt monolayer shell on Pd core nanoparticles, a Cu monolayer was formed on Pd core particles by underpotential deposition (upd), followed by galvanic displacement with Pt to prepare Pd core/Pt shell nanoparticles-loaded carbon black (Pt/Pd/CB) catalysts [9]. The prepared Pt/Pd/CB exhibited high ORR activity per unit mass of Pt (mass activity, MA) [9–11], suggesting that the Pt consumption was highly reduced.

To prepare Pd nanoparticles, various stabilizers like polyvinylpyrrolidone, tetra(*n*-octylammonium) bromide, cetyltrimethylammonium bromide, sodium citrate, oleylamine *etc.* [12–15], have been used so far. However, the removal of the stabilizers is so tiresome that the preparation of Pd nanoparticles without any stabilizer is desirable in terms of low cost and low environmental load. Quite recently, the specific preparation method of Pt/Pd nanoparticles without any stabilizer has been reported although they were not loaded on CB [16]. Recently, we have succeeded in the simple preparation of Pt and Au nanoparticle-loaded CB with relatively narrow size distribution by using CO as a reducing agent [17,18]. In this study, we applied this method to the synthesis of Pd core nanoparticle-loaded CB (Pd/CB), and, consequently, we successfully prepared CB loaded Pd core nanoparticles less than 5 nm in mean size without any stabilizer by bubbling CO in acetonitrile solutions containing palladium acetate. Moreover, after a Pt monolayer shell was formed on the Pd core nanoparticles by upd of Cu and the following galvanic displacement with Pt, the ORR activity was greatly enhanced.

2. Results and Discussion

2.1. Structural Properties of Pd/CB and Pt Monolayer-Modified Pd/CB

Figure 1 shows X-ray diffraction (XRD) patterns of Pd/CB prepared under different conditions. When the concentrations of palladium acetate in acetonitrile was changed from 0.05 to 1.0 mM, CO bubbling time was fixed to 5 min. On the other hand, when CO was bubbled for 3–60 min, the concentration of palladium acetate in acetonitrile was fixed to 1 mM. In all XRD patterns of Figure 1 a broad reflection peak assigned to Pd(111) was distinctly observed at 2θ = *ca.* 40°, suggesting the production of Pd nanoparticles [19], while there were not any peaks assigned to Pd oxides. Figure 2 shows a Pd3d core level spectrum of Pd/CB as the concentration of palladium acetate in acetonitrile was 1 mM and the CO bubbling time was 5 min. The spectrum indicates that only metallic Pd was produced, supporting the XRD data. In Figure 1a, the intensity of the (111) peak was significantly increased as the concentration of palladium acetate in acetonitrile was increased, suggesting the increase in the amount of produced Pd

nanoparticles. In contrast, the increase in the CO bubbling time did not contribute to the increase in the peak intensity, as shown in Figure 1b.

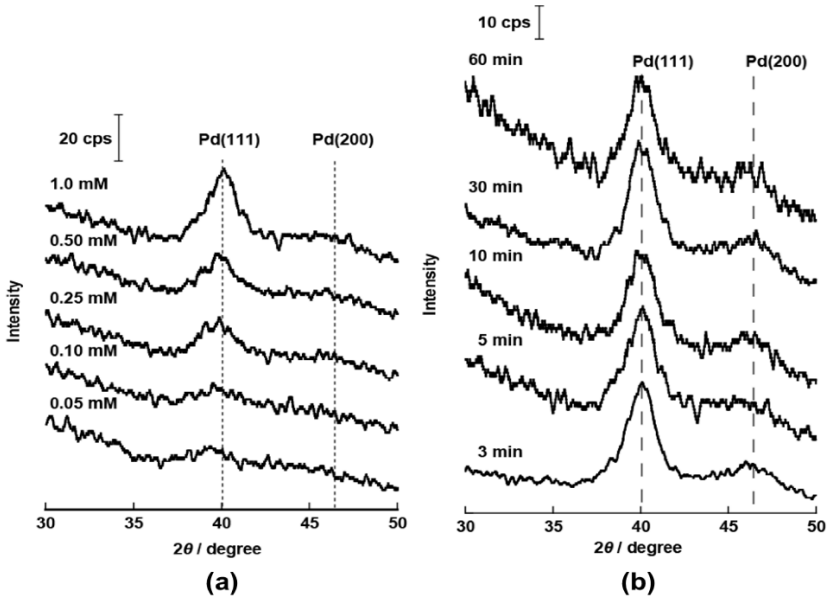

Figure 1. X-ray diffraction patterns of Pd/CB prepared with (**a**) 0.05–1.0 mM palladium acetate in acetonitrile when CO was bubbled for 5 min and (**b**) 1.0 mM palladium acetate in acetonitrile when CO was bubbled for 3–30 min.

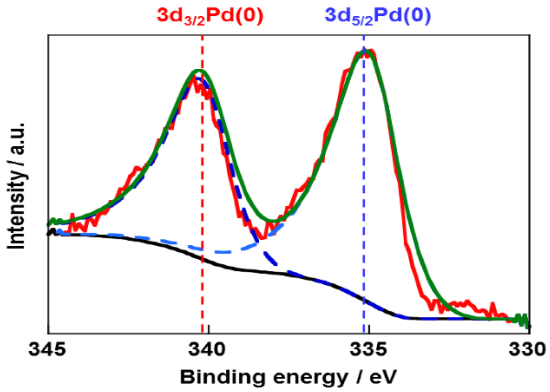

Figure 2. A Pd3d core level spectrum of Pd/CB prepared by bubbling CO in an acetonitrile solution containing 1 mM palladium acetate for 5 min.

The mean size of Pd nanoparticles in the Pd/CB prepared with a variety of the concentration of palladium acetate in acetonitrile and CO bubbling time was estimated by applying the Scherrer's Equation to the (111) peak in each XRD pattern. The results are summarized in Figure 3. In Figure 3a, when the concentrations of palladium acetate in acetonitrile was 0.1 mM or less, the mean size of the prepared Pd nanoparticles was around 3.1 nm, while at more than 0.1 mM it was increased with the concentration of palladium acetate in acetonitrile. This can be ascribed to the growth of the Pd nanoparticles due to the progress of Pd deposition. In Figure 3b, when the CO bubbling time was 10 min or less, the mean particle size was maintained at *ca.* 4.2 nm, while at more than 10 min it was increased with the CO bubbling time. This can be ascribed to the agglomeration of Pd nanoparticles before loading

on the CB powder. From these results, it is concluded that the mean size of Pd nanoparticles can be controlled by the concentration of palladium acetate in acetonitrile and the CO bubbling time, and the former is effective in the preparation of smaller particles. The Pd/CB catalysts prepared by bubbling CO in acetonitrile solutions containing 1.0 and 0.25 mM palladium acetate for 5 min are used hereafter, which are named $Pd_{4.2}$/CB and $Pd_{3.3}$/CB, respectively.

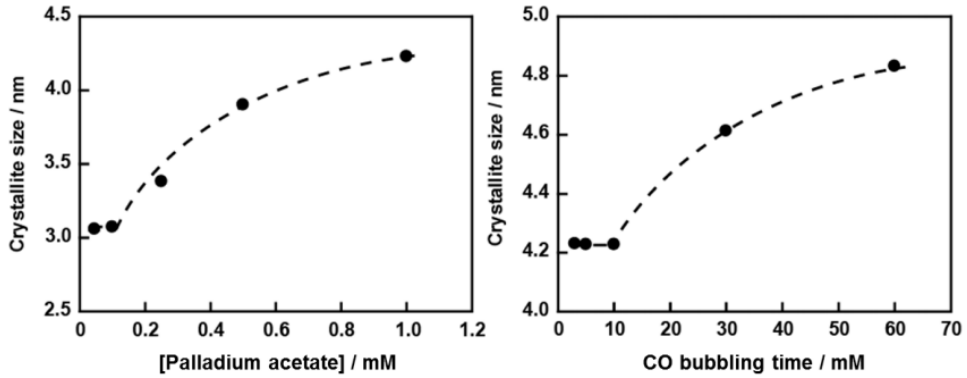

Figure 3. Crystalline size of Pd nanoparticles as a function of (**a**) the concentration of palladium acetate in acetonitrile and (**b**) the CO bubbling time.

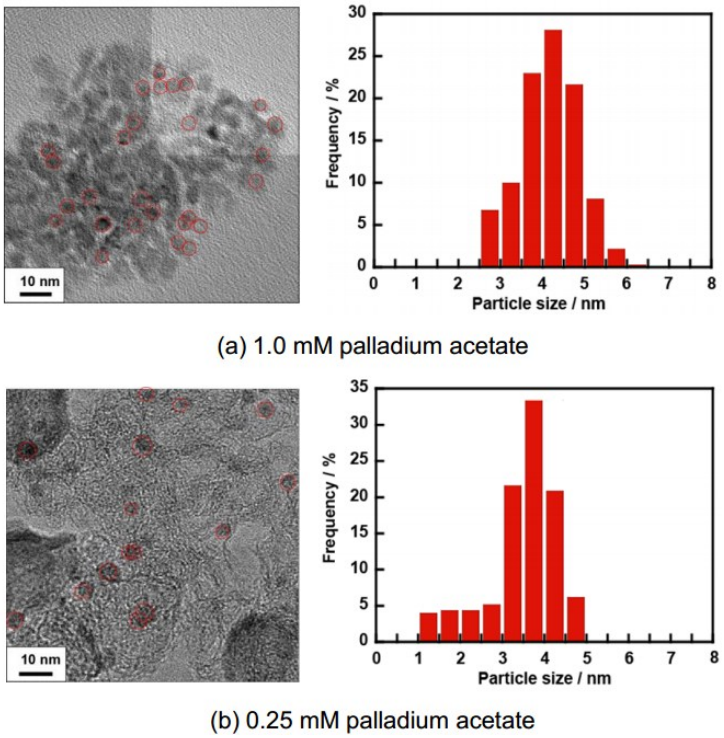

Figure 4. TEM images and histograms of size of Pd nanoparticles loaded on CB prepared by bubbling CO in acetonitrile containing (**a**) 0.25 mM and (**b**) 1 mM palladium acetate for 5 min.

Figure 4 shows TEM images and the histograms of the size of the Pd nanoparticles in $Pd_{4.2}$/CB and $Pd_{3.3}$/CB. The TEM images exhibited that in both cases the Pd nanoparticles were well dispersed on CB. The mean size and standard deviation of the Pd nanoparticles were evaluated to be 3.5 ± 0.9 nm and 4.2 ± 0.7 nm for $Pd_{3.3}$/CB and $Pd_{4.2}$/CB, respectively. In the former, the particles less than 2.5 nm in diameter were included. This seems to be because smaller nuclei are formed at lower precursor

concentrations and their growth rate is slow. In both cases the mean size of the Pd nanoparticles evaluated from XRD and TEM was almost equivalent to each other. In this way, we succeeded in preparing Pd nanoparticles less than 5 nm in diameter without any stabilizer by a simple method in which palladium acetate and CO was used as a precursor and a reducing agent, respectively.

Figure 5 shows the Pt4f and Pd3d core level spectra for the Pt/$Pd_{4.2}$/CB catalyst. Both spectra clearly indicate that both Pd and Pt have the metallic state. With the peak area for Pd and Pt in both spectra, atomic ratio of Pd and Pt (Pd:Pt) was estimated as 0.80:0.20. If a Pd core nanoparticle with the size of 4.2 nm is covered with a Pt monolayer, Pd:Pt = 0.69:0.31. However, since the Pd core nanoparticles are loaded on CB, the contact surface of Pd with CB is dead space, so the fraction of the exposed Pt surface should be less than 0.31. The utilization of Pd for the $Pd_{4.2}$/CB, which is defined by the ratio of electrochemical surface area of 4.2 nm Pd nanoparticles evaluated by CO stripping to the calculated surface area of the same Pd nanoparticles which are assumed to be spherical, was evaluated as 63%. So the ratio of the exposed Pt is estimated as 0.31 × 0.63 = 0.20, and Pd:Pt = 0.80:0.20, which is equivalent to the experimental value. Moreover, the atomic ratio was also equivalent to that evaluated from inductively coupled plasma spectroscopy. This suggests that the Pt shell monolayer almost covered the Pd core nanoparticles.

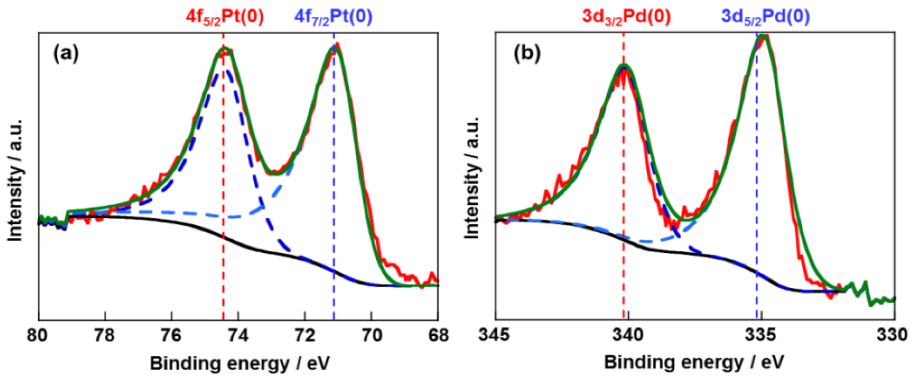

Figure 5. (**a**) Pt4f and (**b**) Pd3d core level spectra for Pt/$Pd_{4.2}$/CB.

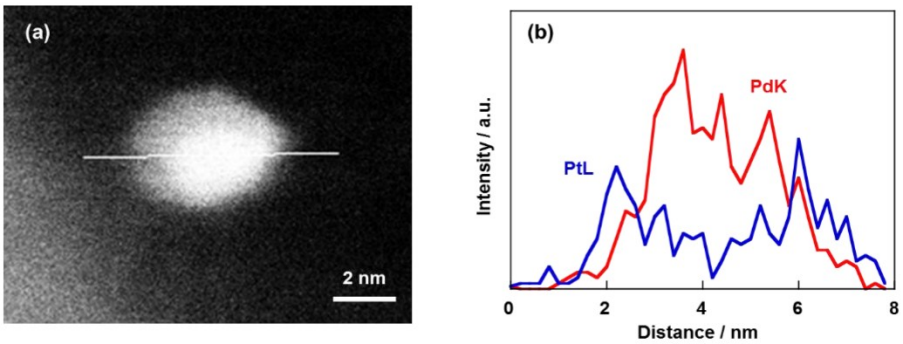

Figure 6. (**a**) A transmission electron micrograph of a $Pt_{4.2}$ core/Pt shell nanoparticle loaded on CB and (**b**) EDX line scan spectra of Pd and Pt.

Figure 6 shows a transmission electron micrograph and its EDX line profile for a 4.2 nm Pd core/Pt shell nanoparticle loaded on CB. Figure 6b exhibited that Pd and Pt were observed over the whole nanoparticle. In particular, the intensity of Pd was high in the center of the nanoparticle, whereas that of

Pt was high at both edges of the nanoparticle, suggesting that the Pd core nanoparticle was covered with Pt.

2.2. Electrochemical Properties of Pt/Pd/CB Electrodes

Figure 7 shows cyclic voltammograms (CVs) of the Pt monolayer-modified $Pd_{4.2}$/CB ($Pt/Pd_{4.2}$/CB), Pt monolayer-modified $Pd_{3.3}$/CB ($Pt/Pd_{3.3}$/CB), $Pd_{4.2}$/CB and $Pd_{3.3}$/CB electrodes in an Ar-saturated 0.1 M $HClO_4$ aqueous solution. The CVs of the $Pd_{4.2}$/CB and $Pd_{3.3}$/CB electrodes had two pairs of redox peaks in the potential range less than 0.4 V in addition to a distinct reduction peak of palladium oxide at *ca.* 0.75 V, which agrees with CVs of the Pd thin layers and Pd nanoparticles [9,20,21]. A couple of large peaks at *ca.* 0.1 V can be assigned to the hydrogen absorption/desorption process in the Pd nanoparticles, while the two small peaks at *ca.* 0.27 V are assigned to the hydrogen adsorption/desorption on the Pd nanoparticles [20].

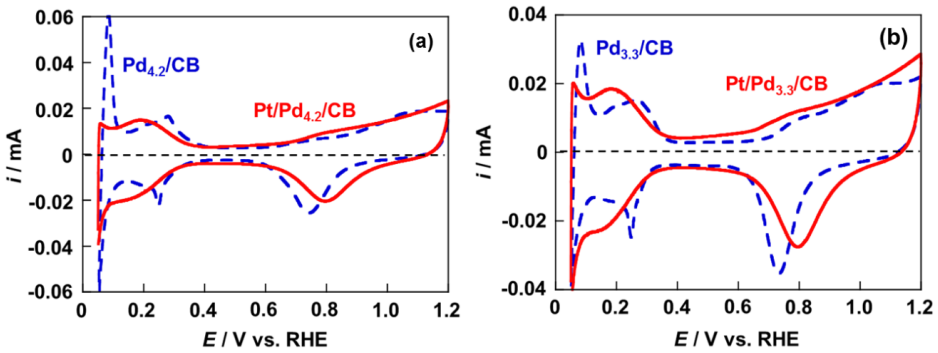

Figure 7. Cyclic voltammograms of (**a**) $Pt_x/Pd_{4.2}$/CB (x = 0, 1) and (**b**) $Pt_x/Pd_{3.3}$/CB (x = 0, 1) electrodes in Ar-saturated 0.1 M $HClO_4$ aqueous solution. Scan rate: 20 mV s^{-1}.

For the $Pt/Pd_{4.2}$/CB and $Pt/Pd_{3.3}$/CB electrodes, two pairs of peaks in the potential range less than 0.4 V almost disappeared, and the peaks assigned to the hydrogen adsorption/desorption (*ca.* 0.2 V) and hydrogen evolution/oxidation (*ca.* 0.05 V) appeared instead. Moreover, the potential of the reduction peak of oxide was shifted more positively [9]. These modifications are ascribable to the phenomena on Pt, suggesting that the Pd nanoparticles were almost covered with a Pt monolayer.

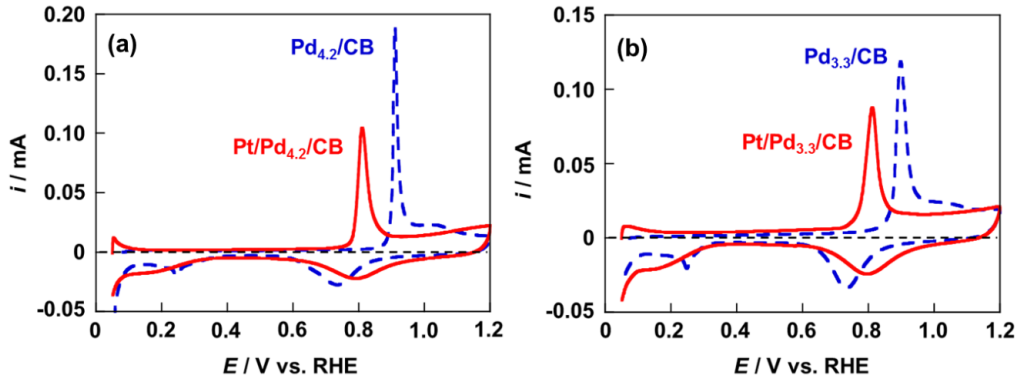

Figure 8. CO stripping voltammograms of (**a**) $Pt_x/Pd_{4.2}$/CB (x = 0, 1) and (**b**) $Pt_x/Pd_{3.3}$/CB (x = 0, 1) electrodes in Ar-saturated 0.1 M $HClO_4$ aqueous solution. Scan rate: 20 mV s^{-1}.

Figure 8 shows CO stripping voltammograms of the $Pt_x/Pd_{4.2}/CB$ (x = 0, 1) and $Pt_x/Pd_{3.3}/CB$ (x = 0, 1) electrodes in Ar-saturated 0.1 M $HClO_4$ aqueous solution. For the $Pd_{4.2}/CB$ and $Pd_{3.3}/CB$ electrodes, the CO stripping peak was observed at *ca.* 0.92 V. Irrespective of the size of Pd nanoparticles, after the deposition of a Pt monolayer, the CO stripping peak significantly shifted in the negative direction, and its potential was quite close to that of Pt. These results also strongly suggest that the Pt monolayer shell almost covers the Pd core nanoparticles.

2.3. Activity and Durability for ORR of Pt/Pd4.2/CB and Pt/Pd3.3/CB Electrodes

Figure 9 shows hydrodynamic voltammograms at various rotating speeds and the Koutecky-Levich plots at various potentials for the $Pt/Pd_{4.2}/CB$ and $Pt/Pd_{3.3}/CB$ electrodes in O_2-saturated 0.1 M $HClO_4$ aqueous solution. As shown in Figure 9b,d, in both cases, there was a linear relationship between the reciprocal of square root of rotating speed ($\omega^{-1/2}$) and the reciprocal of measured current density (i^{-1}) irrespective of potential. With a slope of each straight line and the following Equation (1) [4], the number of electrons in the ORR was evaluated.

$$i^{-1} = i_k^{-1} + (0.62nFc_{O2}D_{O2}^{2/3}v^{-1/6})^{-1}\omega^{-1/2} \quad (1)$$

where i_k is the kinetic current density in mA cm^{-2}, n is the number of electrons in the ORR, F is the Faraday constant, c_{O2} is the dissolved O_2 concentration (1.18×10^{-3} mol L^{-1} [4]), D_{O2} is the diffusion coefficient of O_2 (1.9×10^{-5} cm^2 s^{-1} [4]) and v is the viscosity of the solution (0.0893×10^{-2} cm^2 s^{-1} [4]). In both cases the number of electrons in ORR was evaluated to be *ca.* 4 irrespective of potential, indicating that direct 4-electron reduction reaction to water proceeded on these electrodes, which was the same as the Pt electrode. Moreover, the mechanism of ORR was not influenced by the size of Pd core nanoparticles.

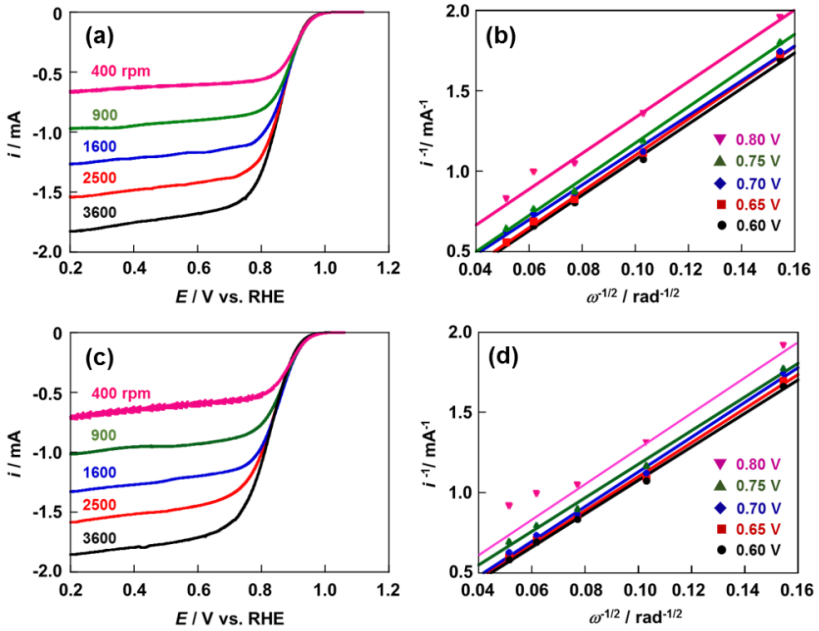

Figure 9. Hydrodynamic voltammograms at various rotating speeds and the Koutecky-Levich plots at various potentials for (**a**,**b**) $Pt/Pd_{4.2}/CB$ and (**c**,**d**) $Pt/Pd_{3.3}/CB$ electrodes in O_2-saturated 0.1 M $HClO_4$ aqueous solution. Scan rate: 10 mV s^{-1}.

i_k can be evaluated using the following Equation (2) [4].

$$i_k = i_l\, i/(i_l - i) \quad (2)$$

where i_l is the diffusion-limited current density and can be determined from Figure 9a,c. Using hydrodynamic voltammograms at 1600 rpm, the log i_k—electrode potential (E) plot or Tafel plot for the Pt/Pd$_{4.2}$/CB and Pt/Pd$_{3.3}$/CB electrodes was made, as shown in Figure 10. The Tafel slopes at the higher (E > 0.85 V) and lower (E < 0.85 V) potential regions was −61 and −120 mV dec^{-1} for the Pt/Pd$_{4.2}$/CB electrode and −63 and −119 mV dec^{-1} for the Pt/Pd$_{3.3}$/CB electrode. The Tafel slope for polycrystalline Pt electrodes was *ca.* −60 and *ca.* −120 mV dec^{-1} at higher and lower potential regions due to the ORR on a Pt surface covered with oxides and a clean Pt surface, respectively [22,23]. Therefore, the ORR mechanism on both Pt/Pd/CB catalysts is the same as that on Pt, and, in particular, the rate-determining step in the lower potential region was the first one-electron reduction reaction of O_2 molecules adsorbed on the Pt surface [22,23].

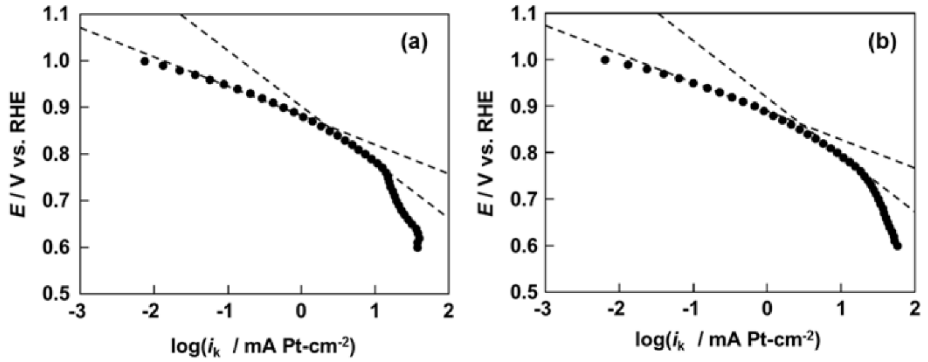

Figure 10. Tafel plots for (**a**) Pt/Pd$_{4.2}$/CB and (**b**) Pt/Pd$_{3.3}$/CB electrodes.

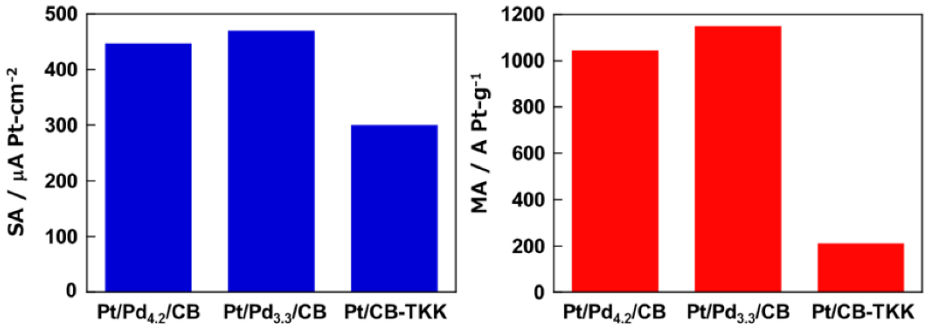

Figure 11. SA and MA for the Pt/Pd$_{4.2}$/CB, Pt/Pd$_{3.3}$/CB and Pt/CB-TKK electrodes.

Figure 11 summarizes the ORR activity per electrochemical surface area of Pt (specific activity, SA) and MA, ORR current per unit mass of Pt at 0.90 V for the Pt/Pd$_{4.2}$/CB, Pt/Pd$_{3.3}$/CB and commercial Pt/CB (TEC10E50E, Tanaka Kikinzoku Kogyo, Oshu-city, Iwate, Japan; Pt/CB-TKK) electrodes. For SA, both Pt/Pd/CB electrodes was about 1.5 times as high as the Pt/CB-TKK electrode, and the Pt/Pd$_{3.3}$/CB electrode whose Pd core size was smaller had higher SA than the Pt/Pd$_{4.2}$/CB electrode. These results can be ascribed to the compressive strain effect of Pd core nanoparticles, which depends on core size and shape, leading to the compression of Pt-Pt distance of the Pt monolayer shell [24–26]. The strain effect induced d-band shift regulates the adsorption properties of rate-determining

intermediates in catalytic processes, so the maximal compression of the Pt-Pt distance must give the highest SA [24–26]. For MA, the Pt/$Pd_{4.2}$/CB and Pt/$Pd_{3.3}$/CB electrodes was 5.0 and 5.5 times as high as the Pt/CB-TKK electrode, respectively. Since the specific surface areas of both Pt/Pd/CB electrodes were similar to each other, the increase in MA is ascribable to the increase in SA.

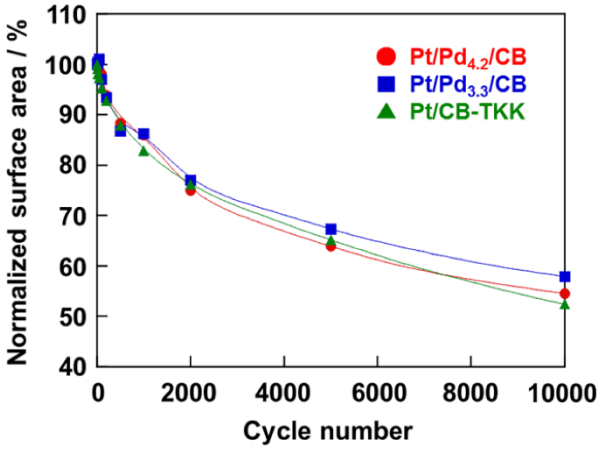

Figure 12. Change in normalized electrochemical surface area of Pt with cycle number for the Pt/$Pd_{4.2}$/CB, Pt/$Pd_{3.3}$/CB and Pt/CB-TKK electrodes.

Figure 12 shows time courses of the normalized ECSA during durability tests at 60 °C for the Pt/$Pd_{4.2}$/CB, Pt/$Pd_{3.3}$/CB and Pt/CB-TKK electrodes. The durability of the Pt/$Pd_{4.2}$/CB and Pt/$Pd_{3.3}$/CB electrodes was comparable to that of Pt/CB-TKK, suggesting that the surface of Pd core nanoparticles was almost covered by Pt atoms for both Pt/Pd/CB electrodes.

3. Experimental Section

3.1. Preparation and Characterization of Pd/CB

The Pd/CB without stabilizer was prepared as follows; CO was bubbled in acetonitrile solutions containing 0.050–1.0 M palladium acetate at 4 °C for 3–60 min, followed by adding Ketjen Black powder and sonicating for 30 min. Then the Pd/CB powder was separated by suction filtration. The loading of Pd on CB was evaluated to be 28 wt% from the mass of the residue by thermogravimetry.

Crystal structure and valence state of Pd/CB were analyzed with an X-ray diffractometer (Shimadzu, Kyoto, Japan; 50 kV, 30 mA) using CuK_α radiation and X-ray photoelectron spectroscope (8 kV, 30 mA) using MgK_α radiation (1253.6 eV). The mean size and its distribution of Pd nanoparticles in Pd/CB were evaluated with a field-emission transmission electron microscope (FE-TEM; Hitachi, Tokyo, Japan). The size distribution profiles were obtained by measuring more than 300 nanoparticles randomly chosen from TEM images.

3.2. Modification of Pd Core Nanoparticles Loaded on CB with Pt Shell

The Pd/CB (Amount of CB: 3.1 μg) was cast on a glassy carbon (GC) disk electrode (5 mmϕ). The Pd/CB-modified GC disk electrode was immersed in a 0.5 M H_2SO_4 aqueous solution containing 2 mM $CuSO_4$ with a Pt plate counter electrode and a reversible hydrogen electrode (RHE). The disk

electrode was polarized at 0.30 V for 10 min to deposit a Cu adlayer on the Pd nanoparticles, followed by being immersed in 5.0 mM K_2PtCl_4 aqueous solution in Ar atmosphere for 30 min. Consequently, a Pt monolayer shell was formed by galvanic displacement of the Cu adlayer atoms with Pt atoms [9]. Each Pd/CB or Pt/Pd/CB electrode was covered with a thin Nafion film by dropping 20 μL of 0.05 wt% Nafion ethanol solution and then drying.

3.3. Electrochemical Measurements

The ORR activity of the Pt/Pd/CB electrodes was measured by hydrodynamic voltammetry using the rotating disk electrode (RDE) technique. The commercial Pt/CB (TEC10E50E, Tanaka Kikinzoku Kogyo, Japan; Pt/CB-TKK) electrode was used for comparison. The counter and reference electrodes were a Pt plate and an RHE, respectively. The electrolyte solution was 0.1 M $HClO_4$. Cyclic voltammograms were recorded at a scan rate of 20 mV s^{-1} in an Ar atmosphere at 25 °C. The hydrodynamic voltammograms were measured at rotating speeds of 3600, 2500, 1600, 900, and 400 rpm in an O_2-saturated 0.l M $HClO_4$ aqueous solution at 25 °C. The potential of the GC disk was swept at 10 mV s^{-1} from 0.05 to 1.2 V. The SA and MA for ORR were evaluated from the kinetic current at 0.90 V *vs.* RHE of each hydrodynamic voltammogram at 1600 rpm, respectively. The mass of Pt deposited on the Pd core nanoparticles for each catalyst was evaluated by integrating the electric charge of the amount of Cu-upd in the stripping voltammogram of the Cu adlayer, assuming that all the Cu adlayer atoms were completely displaced by Pt atoms as follows:

$$Cu + PtCl_4^{2-} \rightarrow Pt + Cu^{2+} + 4Cl^- \quad (3)$$

CO stripping voltammograms were recorded at 20 mV s^{-1} in the positive direction from 0.05 V *vs.* RHE after CO was adsorbed on each electrode at 0.05 V *vs.* RHE in a CO-saturated 0.1 M $HClO_4$ aqueous solution for 15 min.

The durability of Pt/Pd/CB and Pt/CB electrodes was investigated by repeating square-wave potential cycling between 0.6 V for 3 s and 1.0 V for 3 s in an Ar-saturated 0.l M $HClO_4$ aqueous solution at 60 °C [18]. The ECSA of Pt was periodically measured during each durability test, and the loss of the ECSA was used as a measure of degradation.

4. Conclusions

Pd core nanoparticles less than 5 nm in size were successfully prepared without any stabilizer by using palladium acetate as a precursor and CO as a reducing agent. The mean size of Pd nanoparticles was controllable by the concentration of palladium acetate and the CO bubbling time, and the former was superior to the latter in the preparation of smaller particles. The CVs of the Pd/CB electrodes had two pairs of redox peaks in the hydrogen region in addition to a reduction peak of palladium oxide at *ca.* 0.75 V. The deposition of a Pt monolayer shell on CB-loaded Pd core nanoparticles led to the disappearance of the peaks and the appearance of peaks assigned to Pt. The ORR on the $Pt/Pd_{4.2}$/CB and $Pt/Pd_{3.3}$/CB proceeded in 4-electron reduction mechanism like the Pt/CB electrode. The $Pt/Pd_{4.2}$/CB and $Pt/Pd_{3.3}$/CB electrodes was *ca.* 1.5 times higher in SA than the Pt/CB-TKK electrode, and the $Pt/Pd_{3.3}$/CB electrode had higher SA than the $Pt/Pd_{4.2}$/CB electrode. The increase in SA was ascribed to the compression strain effect of the Pd core nanoparticles to tune a Pt-Pt distance which influenced the

adsorption properties of rate-determining intermediates. The MA for the $Pt/Pd_{4.2}/CB$ and $Pt/Pd_{3.3}/CB$ electrodes was 5.0 and 5.5 times as high as that for the Pt/CB-TKK electrode, respectively. The durability of the $Pt/Pd_{4.2}/CB$ and $Pt/Pd_{3.3}/CB$ electrodes was comparable to that of Pt/CB-TKK, suggesting that the surface of Pd core nanoparticles was almost covered by Pt atoms for both Pt/Pd/CB electrodes.

Acknowledgments

This work was supported by the New Energy and Industrial Technology Development Organization (NEDO) through the Industrial Technology Research Grant Program (08002049-0).

Author Contributions

Ryotaro Sakai and Taiki Kuwahara performed the synthesis of catalysts, and the evaluation of loading of metals on CB. Masanobu Chiku carried out the preparation of catalysts-modified electrodes and their electrochemical measurements. Eiji Higuchi performed structural characterization by XRD, XPS and FE-TEM. All the authors contributed equally to the data interpretation and discussion. Hiroshi Inoue coordinated and wrote the manuscript.

Conflicts of Interest

The authors declare no conflict of interest.

References

1. Toda, T.; Igarashi, H.; Uchida, H.; Watanabe, M. Enhancement of the electroreduction of oxygen on Pt alloys with Fe, Ni, and Co. *J. Electrochem. Soc.* **1999**, *146*, 3750–3756.
2. Mukerjee, S.; Srinivasan, S.; Soriaga, M.P.; McBreen, J. Role of Structural and electronic properties of Pt and Pt alloys on electrocatalysis of oxygen reduction: An *in situ* XANES and EXAFS investigation. *J. Electrochem. Soc.* **1995**, *142*, 1409–1422.
3. Greeley, J.; Stephens, I.E.L.; Bondarenko, A.S.; Johansson, T.P.; Hansen, H.A.; Jaramillo, T.F.; Rossmeisl, J.; Chorkendorff, I.; Norskov, J.K. Alloys of platinum and early transition metals as oxygen reduction electrocatalysts. *Nat. Chem.* **2009**, *1*, 552–556.
4. Paulus, U.A.; Wokaun, A.; Scherer, G.G.; Schmidt, T.J.; Stamenkovic, V.; Radmilovic, V.; Markovic, N.M.; Ross, P.N. Oxygen reduction on carbon-supported Pt-Ni and Pt-Co alloy catalysts. *J. Phys. Chem. B* **2002**, *106*, 4181–4191.
5. Paffett, M.T.; Berry, J.G.; Gottesfeld, S. Oxygen reduction at $Pt_{0.65}Cr_{0.35}$, $Pt_{0.2}Cr_{0.8}$ and roughened platinum. *J. Electrochem. Soc.* **1998**, *135*, 1431–1436.
6. Smith, M.C.; Gilbert, J.A.; Mawdsley, J.R.; Seifert, S.; Myers, D.J. *In situ* small-angle X-ray scattering observation of Pt catalyst particle growth during potential cycling. *J. Am. Chem. Soc.* **2008**, *130*, 8112–8113.
7. Salgado, J.R.C.; Antolini, E.; Gonzalez, E.R. Structure and activity of carbon-supported Pt-Co electrocatalysts for oxygen reduction. *J. Phys. Chem. B* **2004**, *108*, 17767–17774.

8. Yano, H.; Kataoka, M.; Yamashita, H.; Uchida, H.; Watanabe, M. Oxygen reduction activity of carbon-supported Pt-M (M = V, Ni, Cr, Co, and Fe) alloys prepared by nanocapsule method. *Langmuir* **2007**, *23*, 6438–6445.
9. Zhang, J.; Mo, Y.; Vukmirovic, M.B.; Klie, R.; Sasaki, K.; Adzic, R.R. Platinum monolayer electrocatalysts for O_2 reduction: Pt monolayer on Pd(111) and on carbon-supported Pd nanoparticles. *J. Phys. Chem. B* **2004**, *108*, 10955–10964.
10. Vukmirovic, M.B.; Zhang, J.; Sasaki, K.; Nilekar, A.U.; Uribe, F.; Mavrikakis, M.; Adzic, R.R. Platinum monolayer electrocatalysts for oxygen reduction. *Electrochim. Acta* **2007**, *52*, 2257–2263.
11. Inaba, M.; Ito, H.; Tuji, H.; Wada, T.; Banno, M.; Yamada, H.; Saito, M.; Tasaka, A. Effect of core size on activity and durability of Pt core-shell catalysts for PEFCs. *ECS Trans.* **2010**, *33*, 231–238.
12. Li, Y.; El-Sayed, M.A. The effect of stabilizers on the catalytic activity and stability of Pd colloidal nanoparticles in the suzuki reactions in aqueous solution. *J. Phys. Chem. B* **2001**, *105*, 8938–8943.
13. Shao, M.; Odell, J.; Humbert, M.; Yu, T.; Xia, Y. Electrocatalysis on shape-controlled palladium nanocrystals: Oxygen reduction reaction and formic acid oxidation. *J. Phys. Chem. C* **2013**, *117*, 4172–4180.
14. Vidal-Iglesias, F.J.; Aran-Ais, R.M.; Solla-Gullon, J.; Garnier, E.; Herrero, E.; Aldaz, A.; Feliu, J.M. Shape-dependent electrocatalysis: Formic acid electrooxidation on cubic Pd nanoparticles. *Phys. Chem. Chem. Phys.* **2012**, *14*, 10258–10265.
15. Mazumdar, V.; Sun, S. Oleylamine-mediated synthesis of Pd nanoparticles for catalytic formic acid oxidation. *J. Am. Chem. Soc.* **2009**, *131*, 4588–4589.
16. Cao, K.; Zhu, Q.; Chen, R. Controlled synthesis of Pd/Pt core shell nanoparticles using area-selective atomic layer deposition. *Sci. Rep.* **2015**, *5*, doi:10.1038/srep08470.
17. Higuchi, E.; Taguchi, A.; Hayashi, K.; Inoue, H. Electrocatalytic activity for oxygen reduction reaction of Pt nanoparticle catalysts with narrow size distribution prepared from $[Pt_3(CO)_3(\mu\text{-}CO)_3]_n^{2-}$ (n = 3–8) complexes. *J. Electroanal. Chem.* **2011**, *663*, 84–89.
18. Higuchi, E.; Hayashi, K.; Chiku, M.; Inoue, H. Simple preparation of Au nanoparticles and their application to Au core/Pt shell catalysts for oxygen reduction reaction. *Electrocatalysis* **2012**, *3*, 274–283.
19. Erdogan, H.; Metin, O.; Ozkar, S. *In situ*-generated PVP-stabilized palladium(0) nanocluster catalyst in hydrogen generation from the methanolysis of ammonia-borane. *Phys. Chem. Chem. Phys.* **2009**, *11*, 10519–10525.
20. Zhang, J.; Qiu, C.; Ma, H.; Liu, X. Facile fabrication and unexpected electrocatalytic activity of palladium thin films with hierarchical architectures. *J. Phys. Chem. C* **2008**, *112*, 13970–13975.
21. Gabrielli, C.; Grand, P.P.; Lasia, A.; Perrot, H. Investigation of hydrogen adsorption and absorption in palladium thin films: II. Cyclic voltammetry. *J. Electrochem. Soc.* **2004**, *151*, A1937–A1942.
22. Damjanovic, A.; Genshaw, M.A. Dependence of the kinetics of O_2 dissolution at Pt on the conditions for adsorption of reaction intermediates. *Electrochim. Acta* **1970**, *15*, 1281–1283.
23. Markovic, N.M.; Ross, P.N. Electrocatalysis as well-defined surfaces: Kinetics of oxygen reduction and hydrogen oxidation/evolution on Pt(*hkl*) electrodes; mechanism of methanol electro-oxidation. In *Interfacial Electrochemistry, Theory, Experiment, and Applications*; Wieckowski, A., Ed.; Marcel Dekker: New York, NY, USA, 1999; pp. 821–841.

24. Hammer, B.; Nørskov, J.K. Theoretical Surface Science and Catalysis—Calculations and Concepts. *Adv. Catal.* **2000**, *45*, 71–129.
25. Wang, J.X.; Inada, H.; Wu, L. ; Zhu, Y.; Choi, Y.; Liu, P.; Zhou, W.−P.; Adzic, R.R. Oxygen reduction on well-defined core-shell nanocatalysts: Particle size, facet, and Pt shell thickness effects. *J. Am. Chem. Soc.* **2009**, *131*, 17298–17302.
26. Wang, X.; Orikasa, Y.; Takesue, Y.; Inoue, H.; Nakamura, M.; Minato, T.; Hoshi, N.; Uchimoto, Y. Quantitating the lattice strain dependence of monolayer Pt shell activity toward oxygen reduction. *J. Am. Chem. Soc.* **2013**, *135*, 5938–5941.